Article

Mechanical and Magnetic Investigations of Balls Made of AISI 1010 and AISI 1085 Steels after Nitriding and Annealing

Sławomir Maksymilian Kaczmarek [1,*], **Jerzy Michalski** [2,*], **Tadeusz Frączek** [2], **Agata Dudek** [2], **Hubert Fuks** [1] **and Grzegorz Leniec** [1]

[1] Department of Technical Physics, Faculty of Mechanical Engineering and Mechatronics, West Pomeranian University of Technology in Szczecin, al. Piastów 48, 70-311 Szczecin, Poland; hubert.fuks@zut.edu.pl (H.F.); grzegorz.leniec@zut.edu.pl (G.L.)

[2] Faculty of Production Engineering and Materials Technology, Czestochowa University of Technology, Al. Armii Krajowej 19, 42-201 Czestochowa, Poland; fraczek.tadeusz@wip.pcz.pl (T.F.); dudek.agata@wip.pcz.pl (A.D.)

[*] Correspondence: skaczmarek@zut.edu.pl (S.M.K.); jerzymichalski987@gmail.com (J.M.)

Abstract: This paper discusses the changes in the phase composition and magnetic properties of the AISI 1010 and AISI 1085 steels that were nitrided at 570 °C in an ammonia atmosphere for 5 h and that were then annealed at 520 °C in a N_2/Ar atmosphere for 4 h. The test samples were made in the form of balls with diameters of less than 5 mm. The thickness of the obtained iron nitride layers was assessed through metallographic tests, while the phase composition was verified through X-ray tests. The magnetic properties were determined using ferromagnetic resonance (FMR) and superconducting quantum interference device (SQUID) techniques. Our research shows that, during the annealing of iron nitrides with a structure of $\varepsilon + \gamma'$, the ε phase decomposes first. As a result of this process, an increase in the content of the γ' phase of the iron nitride is observed. When the ε phase is completely decomposed, the γ' phase begins to decompose. The observed FMR signals did not come from isolated ions but from more magnetically complex systems, e.g., Fe–Fe pairs or iron clusters. Studies have shown that nitriding and annealing can be used to modify the magnetic properties of the tested steels.

Keywords: nitriding of AISI 1010 and 1085 steel balls; annealing in an inert atmosphere; phase composition; white layer; porous zone; magnetic properties; FMR spectra; FMR and SQUID susceptibility

1. Introduction

Nitriding has been used in the engineering industry for many years to improve the wear resistance of machine and tool parts [1,2]. Iron nitrides, in addition to high hardness and corrosion resistance, are characterized by very good magnetic properties. Magnetic materials are used in generators and electric motors as well as electronic and electromechanical devices; they are also used in data carriers. Alloys containing rare earth elements have excellent magnetic properties, so they are most often used in practice [3,4]. Due to limited rare earth metal resources and the intense increase in the demand for magnetic materials, research on magnetic materials without rare earth materials is fully justified. Research on the magnetic properties of iron nitrides meets these needs [5,6].

Iron nitrides belong to an important group of magnetic materials. The iron nitride γ'-Fe$_4$N meets the requirements for soft magnetic materials very well and, at the same time, is resistant to corrosion. The magnetization saturation of γ'-Fe$_4$N is slightly lower (by about 4%) than that of α-Fe, and its coercivity is negligibly small [7,8]. On the other hand, the iron nitride α''-Fe$_{16}$N$_2$ exhibits 30% higher magnetization saturation than α-Fe [9]. Therefore, it is a very good material for high-density magnetic storage media [10]. However, the α''-Fe$_{16}$N$_2$ nitride decomposes to α-Fe and γ'-Fe$_4$N at 200 °C and then completely converts

to α-Fe at 300 °C [11,12]. Its low thermal resistance reduces its attractiveness. On the other hand, the iron nitride γ'-Fe$_4$N, when heated in an inert atmosphere, is stable up to 650 °C [13]. Frączek et al. [14] showed that during the annealing of nitrided layers with the structure $\varepsilon + \gamma'$, which is present in AISI 1085 steel, ε phase decomposition ($\varepsilon \rightarrow \gamma' + \uparrow$) is observed. This takes place after annealing at 520 °C for 5 h in an inert H$_2$/N$_2$ atmosphere at a ratio of 3:1 and a pressure of 200 Pa. After another 5 h, the γ' phase also decomposes ($\gamma' \rightarrow \alpha$-Fe(N) + N$\uparrow$).

Among iron nitrides, the largest range of homogeneity in the Fe-N system is shown by the ε phase with a variable ratio of Fe:N Fe$_{2\text{-}3}$N [15]. Depending on the nitrogen concentration, the nitride ε may have ferromagnetic (ε-Fe$_x$N ($2 < x < 3$)) or paramagnetic (Fe$_2$N) properties [16]. Compared to the α''-Fe$_{16}$N$_2$ nitride, the ε-Fe$_3$N nitride has a much better thermal stability and slightly worse magnetic properties [17].

Since magnetic properties, such as coercivity, remanence, magnetic permeability, the Curie temperature, and saturation magnetization, depend on the nitrogen concentration in the Fe-N phases, the large homogeneity range of the ε phase allows its magnetic properties to be modified over a wide range [18].

The most effective method of producing iron nitrides with an assumed phase composition is gas nitriding. The composition of the obtained iron nitrides depends on the nitriding temperature and the nitrogen potential [19,20]. Arabczyk et al. [21] annealed a nanocrystalline iron catalyst in an NH$_3$/H$_2$ atmosphere at 350 °C with a varying nitrogen potential value during both nitriding and iron nitride reduction. During the process, the authors recorded a change in the magnetic permeability of the created nitride phases. Tests showed that the magnetic permeability of γ'-Fe$_4$N was 1.280 times higher than that of an iron catalyst, while that of ε-Fe$_x$N was more than 3 times lower.

The thermodynamics and kinetics of the nitriding process are exhaustively described in the literature [22,23], which makes controlling the chemical composition of iron nitrides relatively simple.

The aim of our research was to check whether annealing at 520 °C in an inert atmosphere would cause phase transformations of iron nitrides and whether, as a result of the transformations, a loss of mass in the annealed steels would be observed. We also tried to find some changes in the magnetic properties of the studied steel balls which could be attributed to the formation of new phases in the nitride layer region. As the subject of our research, we chose the AISI 1085 and AISI 1010 steels in the form of spherical balls. The balls were first nitrided, and then some of them were annealed. The balls that were thus altered were subjected to mechanical [14] and magnetic [24–26] tests.

2. Materials and Methods

2.1. Materials and Parameters of Nitriding and Annealing

AISI 1010 and AISI 1085 nonalloy steels were used in the tests. The chemical composition of these steels and the dimensions of the samples (SS—initial samples, "non modified") are listed in Table 1.

Table 1. Characteristics of the steels used. D$_k$—ball diameter.

Grade Steel	Sample No.	D$_K$ (mm)	Element Contents in wt.%				
			C	Mn	Si	P	S
AISI 1010	1A; 11	3.97	0.10	0.5	0.1	0.04	0.05
AISI 1085	5A; 15	5.0	0.85	0.9	0.3	0.04	0.05

The steels were subjected to gas nitriding at 570 °C for 5 h; then, half of the samples were annealed at 520 °C for 4 h in N$_2$/Ar atmosphere at 200 Pa. The samples were weighed before and after the annealing process. The accuracy of weight measurement was as much as 10^{-5} g. The parameters of the nitriding and annealing processes are shown in Table 2.

Table 2. Parameters of nitriding and annealing processes.

Sample No.	Parameters of Nitriding				Parameters of Annealing		
	T (°C)	t (h)	Np (atm^{-05})	Inlet Atmosphere	T (°C)	t (h)	Inlet Atmosphere
1A; 5A	570	5	2.5	NH_3	-	-	-
11; 15	570	5	2.5	-	520	4	$N_2/Ar/P$ = 150 Pa

2.2. Metallographic Research

Metallographic tests were carried out on the above-mentioned balls. Grinding the balls to their diameter, a layer of nitrides of actual thickness was observed and measured on metallographic microsection. In addition to the iron nitride layer, called the white layer (WL; its thickness is labeled g_{mp}; see Figure 1a), we also observed and measured the thickness of the porous zone (g_{por}; see Table 3 and comments in 3.1). Figure 1 shows a method for measuring the thickness of the iron nitride layer [14].
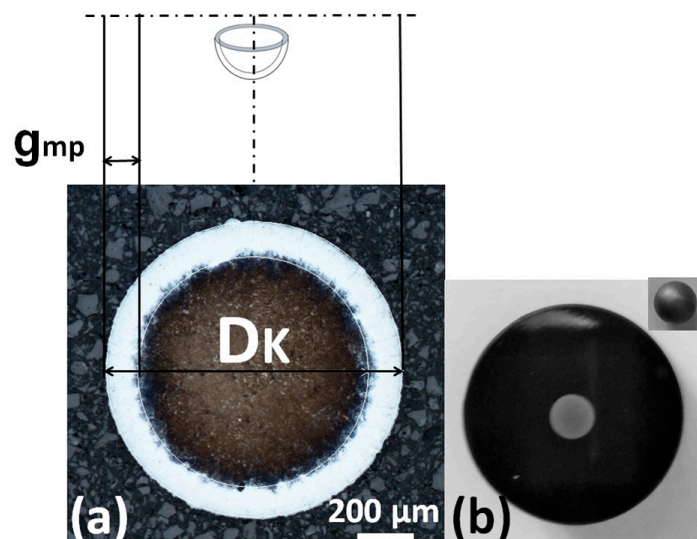

Figure 1. Diagram of measurement of the thickness of the iron nitride layer (WL) of the ball. (**a**) Gray (above) and white (below) surfaces represent the iron nitride layer, g_{mp} represents the actual thickness of the iron nitride layer (WL), and D_K represents ball diameter. (**b**) Metallographic section and appearance of the ball.

The ball diameters and thicknesses of the iron nitride layer and porous zone, observed after nitriding and annealing, are shown in Table 3.

Table 3. Sample geometry after nitriding and annealing.

Grade Steel	Sample No.	D_K (mm)	g_{mp} (μm)	g_{por} (μm)
AISI 1010	1A	3969	29 ± 1	10 ± 1
AISI 1010	11	3969	30 ± 1	12 ± 1
AISI 1085	5A	5.0	25 ± 1	10 ± 1
AISI 1085	15	5.0	25 ± 1	10 ± 1

g_{mp}—nitride layer thickness, g_{por}—thickness of the porous zone, and D_K—ball diameter.

The results of the structural X-ray examination, including the phase composition of the WL as well as the network parameters of the identified iron nitrides and their percentages in WL after nitriding and annealing, are presented in Table 4.

Table 4. The phase composition of the WL and network parameters of iron nitrides.

Grade Steel	Sample No.	PC WL	LP Fe_4N (Å) a = b = c	LP $Fe_{2-3}N$ (Å) a = b	c	PC WL (%) Fe_4N	$Fe_{2-3}N$
AISI 1010	1A	Fe_4N-γ'; $Fe_{2-3}N$-ε	3.7986	4.6932	4.3783	4 ± 2	95 ± 2
AISI 1010	11	Fe_4N-γ'	3.8007	-	-	97 ± 2	-
AISI 1085	5A	Fe_4N-γ'; $Fe_{2-3}N$-ε	3.7978	4.6842	4.3750	13 ± 2	87 ± 2
AISI 1085	15	Fe_4N-γ'; $Fe_{2-3}N$-ε	3.7963	4.6998	4.3817	39 ± 2	61 ± 2

g_{mp}—WL thickness, g_{por}—thickness of the porous zone, LP—lattice parameter, and PC WL—white-layer phase composition.

2.3. Magnetic Resonance Experiment

FMR absorption spectra were recorded in the temperature range of 82–300 K using the conventional X-band spectrometer ELEXSYS E500 (BRUKER, Billerica, MA, USA) operating at f = 9.46 GHz and p = 0.62 mW of microwave power. The first derivative of the absorption spectrum was recorded as a function of the applied magnetic induction, B, which ranged from 0 to 1.4 T. The FMR susceptibility, χ_{FMR}, was calculated as a double integral of the FMR absorption spectrum depending on the temperature. The square of magnetic moment, proportional to the $\chi_{FMR} \times T$ product, and the effective position of the FMR resonant line, g_{eff}, were also analyzed. g_{eff} values were calculated from the B_{res} resonant field and the f_{res} resonant frequency using the resonance condition (g_{eff} = 71.44773 f_{res}(GHz)/B_{res}(mT)).

Static magnetic susceptibility measurements were made with the MPMS-XL7 SQUID (superconducting quantum interference device) magnetometer. Measurements were recorded in the temperature range of ~50 K to room temperature at a magnetic field of 100 Oe. Hysteresis loops were also measured to find other magnetic properties, such as H_c, coercive field, and B_r, remnant parameters.

3. Results

3.1. Phase Transformations of Iron Nitrides

On the AISI 1010 steel (sample 1A), a layer of iron nitrides with a thickness of g_{mp} = 29 ± 1 μm was formed in the nitriding process (see Table 3). In this layer, one can distinguish a lighter zone with poor etching on the substrate and a porous etching zone on the surface with a thickness of g_{por} = 10 ± 1 μm (Figure 2a).

On the diffractogram of the surface of the nitrided sample (1A), the dominant phase in the layer was the ε phase; all the characteristic lines from the ε phase were recorded in the range of the 2Θ angles studied (Figure 2b). The low intensity and the absence of the characteristic lines of the γ' {200} and γ' {111} planes indicate that the amount of the γ' phase in the layer did not exceed 5% of the mass (see Table 4).

After the annealing process, the steel structure (sample 11) did not change significantly. In the microstructure, a layer of iron nitrides with a thickness of g_{mp} = 30 ± 1 μm was visible. The thickness of the light, poorly digestible zone decreased slightly; the thickness of the porous zone (g_{por}) increased to 10 ± 1 μm, and its porosity also increased (Figure 2c). The process significantly changed the phase composition of the iron nitride layer. After the nitriding process, the iron nitride layer was a mixture of ε and γ' phases; after the annealing process, as a result of denitrification, the iron nitride layer was transformed into a single-phase γ' layer. On the diffractogram of the surface of sample 11, only two characteristic lines of γ' {111} and γ' {200} and characteristic lines of the substrate, α-Fe {110}, were identified (Figure 2d). As a result of the transformation, the lattice parameters of the formed γ'-Fe_4N nitride also increased (Table 4). The appearance of a characteristic line of the α-Fe substrate may be associated with the disappearance of part of the nonporous zone of the iron nitrides.
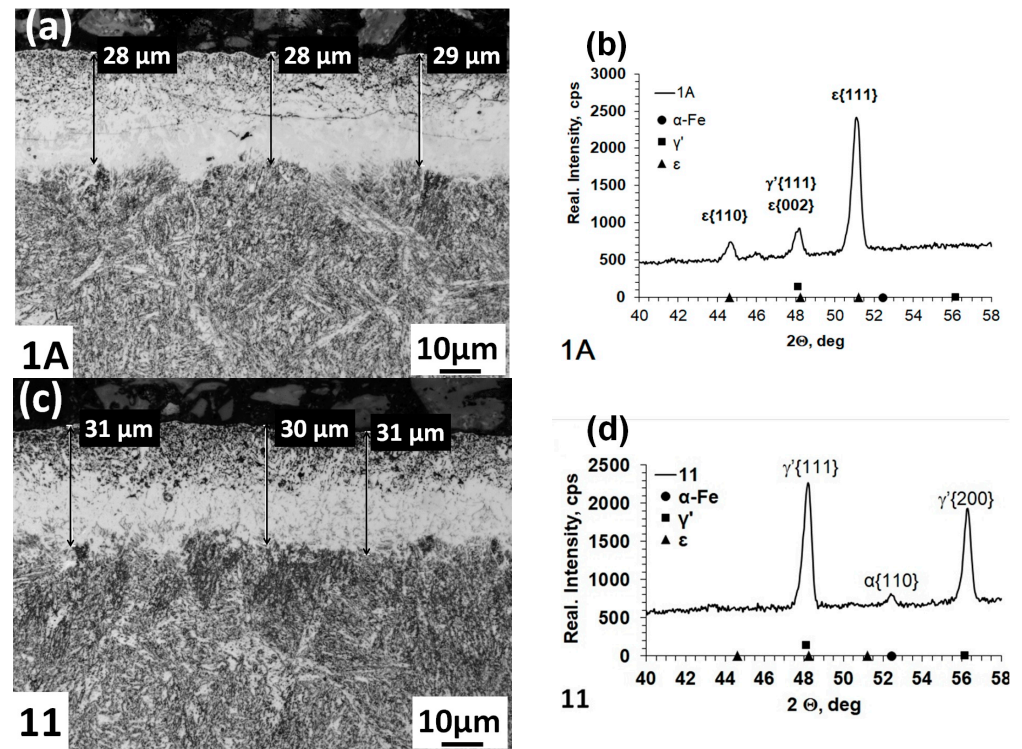
Figure 2. Microstructure of the nitrided layer on AISI 1010 steel (sample 1A) (**a**) and nitrided and annealed steel (sample 11) (**c**). Diffractograms of the surface of nitrided sample (sample 1A) (**b**) and nitrided and annealed sample (sample 11) (**d**).

On the AISI 1085 steel (sample 5A), a layer of iron nitrides with a thickness of $g_{mp} = 25 \pm 1$ µm was formed in the nitriding process (Table 3); in this layer, a lighter zone with poor etching on the substrate and a more etched porous zone with a thickness of $g_{mp} = 10 \pm 1$ µm on the surface can be distinguished (Figure 3a). On the diffractogram of the surface of the nitride sample (5A), the predominant phase in the nitride layer was the ε phase (Figure 3b); the content of the ε phase in the iron nitride layer was 87% (Table 4). All the characteristic lines of the ε phase in the range of the 2Θ angles were tested. The low intensity of the characteristic line of the γ' {111} plane and the low intensity of the characteristic line of the γ' {200} plane indicate that the amount of the γ' phase in the layer did not exceed 15% by weight.
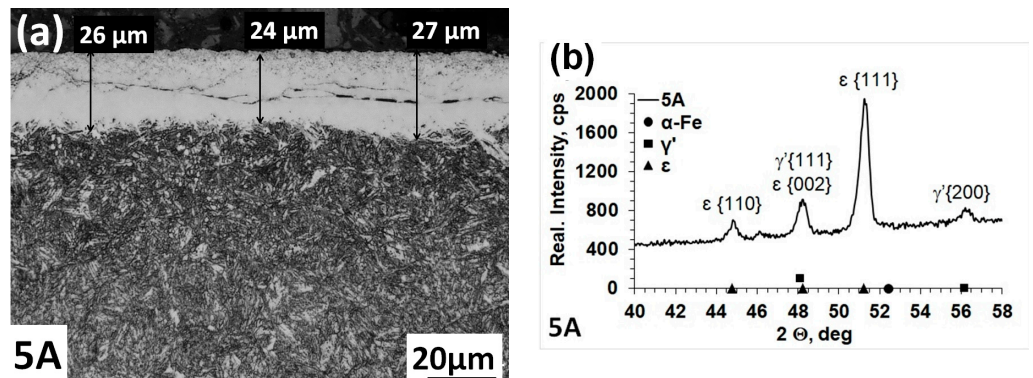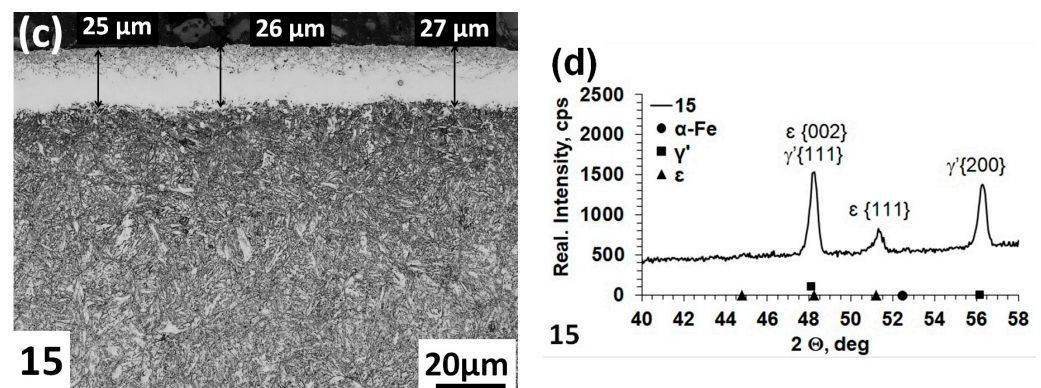

Figure 3. *Cont.*

Figure 3. Microstructure of the nitrided layer on AISI 1085 steel (sample 5A) (**a**) and nitrided and annealed steel (sample 15) (**c**). Diffractograms of the surface of nitrided sample (sample 5A) (**b**) and nitrided and annealed sample (sample 15) (**d**).

After the annealing process, the steel structure (sample 15) did not change significantly. In the microstructure, there was a layer of iron nitrides with a thickness of $g_{mp} = 25 \pm 1$ μm (Table 3). The thickness of the light, poorly etched zone decreased slightly, while the thickness of the porous zone (g_{por}) increased to 12 ± 1 μm (Figure 3c). The degree of porosity of the zone increased. The process significantly changed the phase composition of the iron nitride layer. After the nitriding process, the iron nitride layer was a mixture of ε and γ′ phases. During annealing, only part of the ε phase evolved into the γ′ phase according to the $\varepsilon \rightarrow '\varepsilon + N\uparrow$ reaction, so the iron nitride layer was a mixture of $\varepsilon + \gamma' + \gamma'_\varepsilon$ phases. In the iron nitride layer, next to the γ′ phase formed by the nitriding process, there was also a γ'_ε phase formed as a result of the ε phase transformation (Figure 3d). X-ray studies of sample 15 found that the characteristic line of the ε {110} plane disappeared. The intensity of the ε {111} line decreased significantly; the intensity of the γ′ {200} line and the intensity of the lines of the γ′ {111} and ε {002} planes increased. In the doublet of these phases, the number of γ′ phases increased. As a result of the $\varepsilon\text{-Fe}_{2-3}\text{N}$ phase transformation, the content of the $\gamma'\text{-Fe}_4\text{N}$ phase in the white layer increased. The lattice parameters of γ′ phase increased slightly; the lattice parameters of the ε phase decreased (Table 4).

Figure 4 shows the change in the mass of the annealed samples after the nitriding process. The disappearance of the ε phase and the partial dissociation of the γ′ phase ($\gamma' \rightarrow \alpha\text{-Fe(N)}$) explain the large weight loss in sample 11 (Figure 2d). The incomplete phase transformation of ε to γ′ explains, in turn, the small loss of mass in sample 15 (Figure 3).
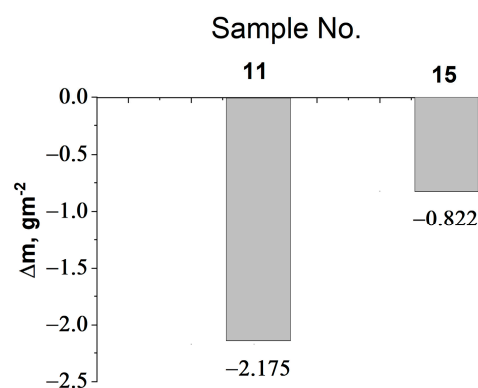

Figure 4. Change in sample weight, $\Delta m / m^2$ (samples 11 and 15), after annealing.

3.2. FMR Spectra

Investigations of the magnetic properties of AISI 1010 steel balls were carried out earlier in this paper [27]. However, these balls were subjected to nitriding processes under

different thermodynamic conditions and ball diameters. The results of these and current studies confirm the independence of the conclusions about the magnetic properties of the balls with respect to their materials and geometric sizes. The magnetic properties of 1085 steel balls were analyzed by us for the first time. By analyzing the general shape of the resonant lines from Figures 5 and 6, it can be seen that "unmodified" (SS) ball materials usually have a very complex, wide, and intense FMR signal observed over the entire available temperature range of 50–300 K, which is far from the standard Lorentzian function (see Figures 5a–c and 6a,b). The AISI 1085 ball samples (SS—initial sample, 5A—nitrided sample, and 15—nitrided and annealed sample) had a diameter of 5 mm and were not suitable for measuring the temperature dependencies of the FMR spectra (diameter was too large in relation to the measuring chamber). Therefore, Figure 6a shows the FMR spectra of a ball cut from the same material but with a different diameter: AISI 1085_SS_2.5 mm. Figure 6b shows only the FMR spectra of the AISI_1085_5 mm samples measured at room temperature. The general characteristics of the spectra shown in Figure 6a correspond to those shown in Figure 6b.

Let us assume for our samples the correctness of the model of isolated Fe ions. The asymmetry of the FMR resonant signal can be explained by the very high conductivity of steel, leading to the formation of skin currents in the FMR experiment. Such a phenomenon was first described by Dyson [24] and was studied in further FMR experiments [25,26]. According to this theory, the symmetric Lorentz line is distorted due to the uneven distribution of the microwave field in the sample. The level of asymmetry, among many factors, depends on the relationship between the size of the sample and the depth of the skin current. The contribution of the asymmetric Dyson function to the overall FMR line is expected to be weaker for samples with a smaller diameter. Thermal treatment (nitriding, annealing) leads to an increase in the homogeneity of the magnetic material, which can be inferred from the increase in the symmetry of the observed FMR signal compared to the signal of the unmodified samples.

In the a–c inserts in Figure 5, the temperature dependencies of the FMR spectra of the AISI 1010 samples are shown for the initial sample (SS), the nitrided sample (1A), and the nitrided and annealed sample (11), respectively. As you can see, the shape and intensity of the FMR signal changed significantly when another process was used (compare Figure 5a–c). Moreover, it changed with increasing temperature.
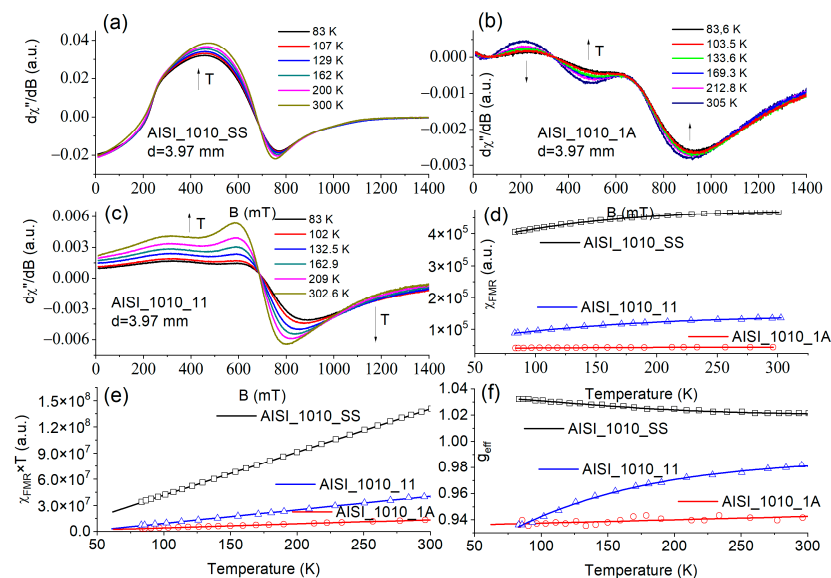

Figure 5. FMR spectra of the AISI_1010 sample; d = 3.97 mm. (**a**–**c**) Temperature dependence of FMR spectra of initial sample (SS), nitrided sample (1A), and nitrided and annealed sample (11), respectively; (**d**–**f**) temperature dependencies of the FMR magnetic susceptibility, χ_{FMR}; magnetic moment square, $\chi_{FMR} \times T$; and FMR signal resonant position, g_{eff}, respectively.

The d–f inserts in Figure 5 show the temperature dependencies of the FMR magnetic susceptibility, χ_{FMR}; the magnetic moment square, $\chi_{FMR} \times T$; and the FMR signal resonant position, respectively. The FMR magnetic susceptibility of all the samples (d) increased with temperature, although higher values were observed for the SS sample. This behavior was completely inconsistent with the Curie–Weiss relationship expected for simple paramagnetic species. The magnetic moments (e) decreased as the temperature decreased, suggesting antiferromagnetic interactions dominating the magnetic behavior of the samples. The resonant position of the FMR line (f) moved towards lower values for both of the nitrided and annealed samples.

The inserts in Figure 6a,c–e show the same relationships as those in Figure 5, but the magnetic susceptibility, magnetic moment, and resonance position are shown for the AISI 1085_SS_2.5 mm sample and not the AISI 1085_SS_5 mm sample. The FMR spectra of the second type of samples (SS, 5A, and 15) measured at T = 295 K are shown in Figure 6b.
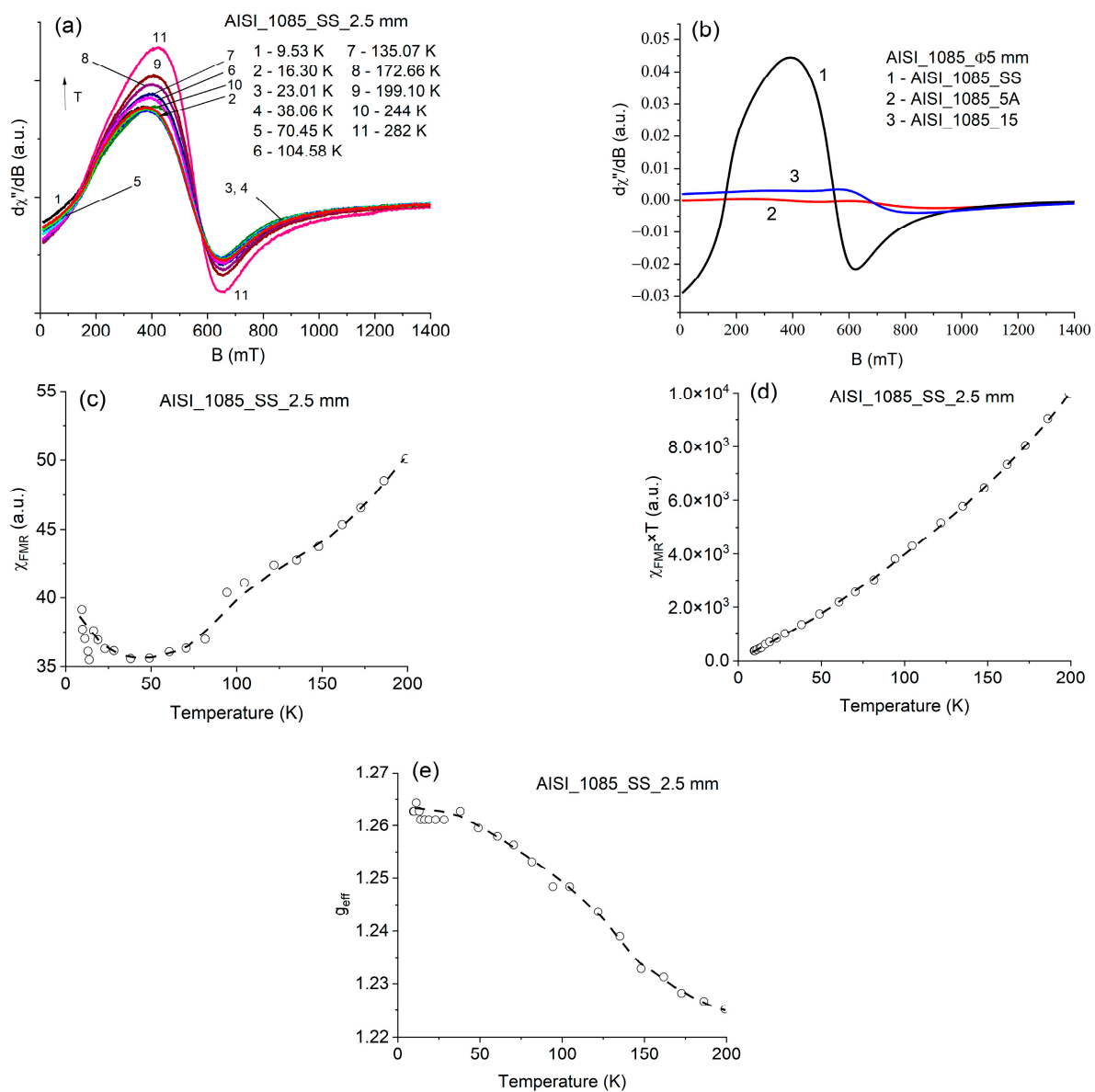

Figure 6. (**a**) The FMR spectra of the AISI 1085_SS_2.5 mm sample at several temperatures, (**b**) the FMR spectra of AISI 1085_SS_5 mm samples (SS, 5A, and 15) measured at room temperature, (**c**) χ_{FMR} of the AISI_11085_SS_2.5 mm sample, (**d**) $\chi_{FMR} \times T$ of the AISI_11085_SS_2.5 mm sample, and (**e**) g_{eff} of the AISI_11085_SS_2.5 mm sample.

Although the above temperature relationships (Figures 5 and 6) were obtained only in the range of 50–300 K, our previous tests in the range of 3–300 K [27] on the same samples tested for something different than the thermodynamical conditions confirmed the above conclusions. The question arises whether and how the nitriding process physically affected the magnetic properties of the tested steel ball samples. As can be seen in Figures 5 and 6, the nitriding process introduced a broad component into the FMR spectra. This component may be the result of the growth of a new phase, e.g., Fe_4N-γ' (see Table 3), which modified the surface of the ball at a different depth. In addition, the thermal nitriding processes led to a change in the shape of the FMR signal. This refers to various conditions, including the relaxation processes between the magnetic centers. On the one hand, the FMR signals recorded for the samples undergoing nitriding processes were transferred to higher magnetic fields, but, at the same time, they became more symmetrical and closer to the shape of the Lorentz line. This clearly suggests that both the temperature and the time of exposure to the nitrogen atmosphere had an impact on the magnetic properties of the tested steel materials. The observed shift of the resonant lines (g_{eff}) towards higher fields can be attributed to the decrease in the electron conductivity of the samples after the nitriding process. The nitriding process generally led to a decrease in the free-electron asymmetric Dysonian component in the FMR spectra. Thus, the general FMR signal consisted of a free-electron FMR signal (Dysonian-like) and a Lorentzian-like FMR signal assigned to the magnetic complexes.

3.3. Magnetic Susceptibility Measurements

Figure 7a, b shows the magnetization measurements of the initial samples, SS, of the AISI 1010 and AISI 1085 steels in a magnetic field of 100 Oe. As can be seen, the samples are characterized by high magnetic anisotropy at lower temperatures and an unusual dependence on temperature over the entire temperature range of 3–300 K. This confirms the previous FMR observations (see Figures 5d and 6c). Magnetic anisotropy tended to disappear at a temperature of about 300 K. Measurements were made in the FC and ZFC modes. For the tested samples, their magnetization was relatively weaker when the tests were carried out in a stronger magnetic field. Moreover, the magnetic susceptibility of this type of steel appears to be dependent on the carbon content.
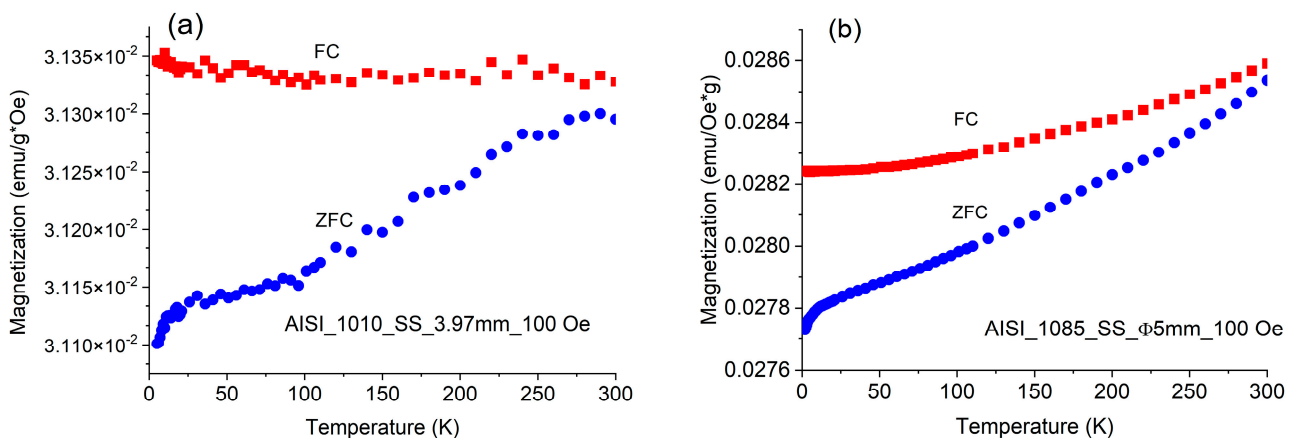

Figure 7. (**a**). Magnetization of the AISI 1010_SS sample over a temperature range of 3–300 K in a magnetic field of H = 100 Oe. (**b**) Magnetization of the AISI 1085_SS sample over a temperature range of 3–300 K in a magnetic field of H = 100 Oe.

Thus, the results obtained from the SQUID measurements, recording changes in magnetization, confirm the remarkable increase in magnetization with increasing temperature previously observed in the FMR measurements.

Figure 8 shows the hysteresis loops measured at 295 K. As you can see, they were very thin. They had a low coercive field, H_c, and low remnant parameters, B_r. They did

not differ much from each other. Figure 8 indicates that all the tested samples revealed (anti)ferromagnetic interactions, regardless of the type of process, over the temperatures of 15–295 K. Only minor differences were observed for different processes. An increase in magnetization, as well as in FMR magnetic susceptibility, along with temperature can be observed in the antiferromagnetic structure. According to previous reports on a similar type of steel [28], we are dealing with a magnetic material, where a minority of ferromagnetic objects appear as an imperfection of the antiferromagnetic structure. Thus, the increase in temperature destroyed the antiferromagnetic order, and the overall magnetization increased. A similar behavior of magnetization with temperature dependence was observed in other materials containing Fe [29,30], where the increase in magnetization was explained by the formation of Fe^{2+} ions in a structure made of Fe^{3+}.
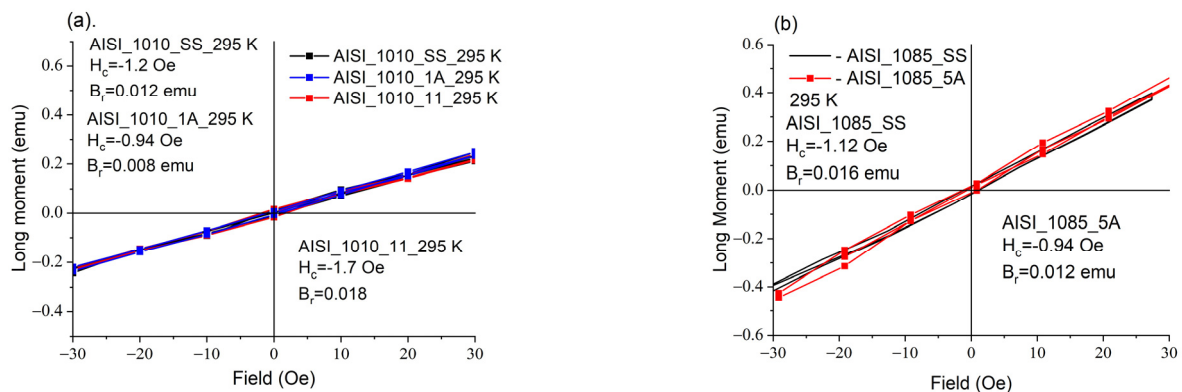

Figure 8. (**a**) Hysteresis loops of the AISI 1010 samples and (**b**) hysteresis loops of AISI 1085 samples; T = 295 K.

4. Conclusions

Our research shows that the iron nitrides formed during nitriding dissociated during annealing at 520 °C in an N_2/Ar atmosphere at 150 Pa. The ε phase was the first to dissociate according to the reaction $\varepsilon \rightarrow \gamma' + N_2\uparrow$. After complete ε phase decomposition, the γ' phase was also decomposed according to reaction $\gamma' \rightarrow \alpha Fe(N) + N_2\uparrow$. The nitrogen released during the dissociation of the iron nitrides caused a loss of mass in the annealed samples. The nitrogen released during the decomposition of the iron nitrides did not change the thickness of the iron nitride layer.

The FMR technique was sensitive enough to record the differences in the physical properties of the AISI steels subjected to different types of nitriding and annealing processes. The samples with a higher carbon content had more symmetrical FMR signals. This was assigned to the share of free electrons in the FMR line shape. Free electrons were observed as a Dyson line in the FMR spectra. In addition to the above line, the usual Lorentz line was observed and was attributed to iron complexes.

Our innovative methodology for investigating the changes in the magnetic properties of steel by observing the mechanical changes in the WL thickness combined with observations of the temperature dependencies of the FMR spectra of the spherical balls turned out to be a valid methodology independent of the type of steel tested; the geometric dimensions of the balls; and the heat treatment processes, including nitriding.

Author Contributions: Conceptualization, S.M.K., J.M. and T.F.; methodology, S.M.K. and J.M.; software, A.D. and G.L.; validation, J.M., S.M.K. and T.F.; formal analysis, S.M.K., J.M., T.F. and G.L.; investigation, S.M.K., A.D., T.F. and G.L.; resources, T.F.; data curation, S.M.K., A.D., H.F. and G.L.; writing—original draft preparation, S.M.K. and J.M.; writing—review and editing, S.M.K. and J.M.; visualization, S.M.K. and J.M.; supervision, S.M.K.; project administration, S.M.K., J.M. and T.F.; funding acquisition, S.M.K., A.D. and T.F. All authors have read and agreed to the published version of the manuscript.

References

1. Borgioli, F. The Corrosion Behavior in Different Environments of Austenitic Stainless Steels Subjected to Thermochemical Surface Treatments at Low Temperatures: An Overview. *Metals* **2023**, *13*, 776. [CrossRef]
2. Godec, M.; Ruiz-Zepeda, F.; Podgoenik, B.; Donik, C.; Kocijan, A.; Balantic, D.A.S. The influence of the plasma-nitriding temperature on the microstructure evolution and surface properties of additive-manufactured 18Ni300 maraging steel. *Surf. Coat. Technol.* **2022**, *4333*, 12808. [CrossRef]
3. Sah, J.V.; Dwivedi, P.K.; Mukherjee, S.; Jhala, G.; Joseph, A. Influence of $\gamma_N{}'$ and $\varepsilon_N{}'$ phases on the properties of AISI 304L after low-temperature plasma nitrocarburizing. *J. Vac. Sci. Technol. A* **2023**, *41*, 33101. [CrossRef]
4. Hono, K.; Sepehri-Amin, H. Strategy for high-coercivity Nd–Fe–B magnet. *Scr. Mater.* **2012**, *67*, 530–535. [CrossRef]
5. Gupta, P.; Fiedler, H.; Rubanov, S.; Kennedy, J. Magnetisation and magnetic anisotropy of ion beam synthesized iron nitride. *J. Magn. Magn. Mat.* **2021**, *517*, 167388. [CrossRef]
6. Zhai, Y.; Zhu, D.; Duan, S.; Luo, F. Novel $Fe_{3\text{-}4}N$@FCI particles with improved microwave absorption and antioxidation properties prepared by surface nitridation method. *Chem. Phys. Lett.* **2020**, *755*, 137803. [CrossRef]
7. Wojciechowski, P.; Lewandowski, M. Iron Nitride Thin Films: Growth, Structure, and Properties. *Cryst. Growth Des.* **2022**, *22*, 4618–4639. [CrossRef]
8. Yamaguchi, T.; Sakita, M.; Nakamura, M.; Kobira, T. Synthesis and Characteristics of Fe_4N Powders and Thin Films. *J. Magn. Magn. Mater.* **2000**, *215–216*, 529–531. [CrossRef]
9. Liu, J.; Guo, G.; Zhang, F.; Wu, Y.; Ma, B.; Wang, J.-P. Synthesis of α''-$Fe_{16}N_2$ Ribbons with a Porous Structure. *Nanoscale Adv.* **2019**, *1*, 1337–1342. [CrossRef]
10. Wang, X.; Zheng, W.T.; Tian, H.W.; Yu, S.S.; Xu, W.; Meng, S.H.; He, X.D.; Han, J.C.; Sun, C.Q.; Tay, B.K. Growth, Structural, and Magnetic Properties of Iron Nitride Thin Films Deposited by DC Magnetron Sputtering. *Appl. Surf. Sci.* **2003**, *220*, 30–39. [CrossRef]
11. Zheng, Q.; Yu, M.; Wen, W.; Liu, S.; Liang, X.; Wang, C.; Dai, Y.Y.; Xu, Y. Porous and flake-like γ' -Fe_4N@iron oxides with enhanced microwave absorption performance. *Ceram. Internat.* **2021**, *47*, 8315–8321. [CrossRef]
12. Jiang, H.; Tao, K.; Li, H. The thermostability of the $Fe_{16}N_2$ phase deposited on a GaAs substrate by ion-beam-assisted deposition. *J. Phys. Condens. Matter* **1994**, *6*, L279. [CrossRef]
13. Yurovskikh, A.S.; Kardonina, N.I.; Kolpakov, A.S. Phase transformations in nitrided iron powders. *Met. Sci. Heat Treat.* **2015**, *57*, 507–514. [CrossRef]
14. Frączek, T.; Michalski, J.; Kucharska, B.; Opydo, M.; Ogorek, M. Phase transformations in the nitrided layer during annealing under reduced pressure. *Arch. Civ. Mech. Eng.* **2021**, *21*, 48. [CrossRef]
15. Liapina, T.; Leineweber, A.; Mittemeijer, E.J.; Kockelmann, W. The lattice parameters of ε-iron nitrides: Lattice strains due to a varying degree of nitrogen ordering. *Acta Mater.* **2004**, *52*, 173–180. [CrossRef]
16. Gupta, M.; Tayal, A.; Gupta, A.; Gupta, R.; Stahn, J.; Horisberger, M.; Wildes, A. Iron and Nitrogen Self-diffusion in Non-Magnetic Iron Nitrides. *J. Appl. Phys.* **2011**, *110*, 123518. [CrossRef]
17. Lei, X.; Wang, J.; Peng, R.; Wang, W. The controllable magnetic properties of Fe_3N nanoparticles synthesized by a simple urea route. *Mat. Res. Bull.* **2020**, *122*, 110662. [CrossRef]
18. Robbins, M.; White, J.G. Magnetic properties of epsilon-iron nitride. *J. Phys. Chem. Solids* **1964**, *25*, 717–720. [CrossRef]
19. Kucharska, B.; Michalski, J.; Wójcik, G. Mechanical and microstructural aspects of C20-steel blades subjected to gas nitriding. *Arch. Civ. Mech. Eng.* **2019**, *19*, 147–156. [CrossRef]
20. Michalski, J.; Tacikowski, J.; Wach, P.; Lunarska, E.; Baum, H. Formation of single-phase layer of γ'-nitride in controlled gas nitriding. *Met. Sci. Heat Treat.* **2005**, *47*, 516–519. [CrossRef]
21. Arabczyk, W.; Pelka, R.; Kocemba, I.; Brzoza-Kos, A.; Wyszkowski, A.; Lendzion-Bieluń, Z. Study of Phase Transformation Processes Occurring in the Nanocrystalline Iron/Ammonia/Hydrogen System by the Magnetic Permeability Measurement Method. *J. Phys. Chem. C* **2022**, *126*, 7704–7710. [CrossRef]
22. Małdziński, L. *Termodynamiczne i Technologiczne Aspekty Wytwarzania Warstwy Azotowanej na Żelazie i Stalach w Procesach Azotowania Gazowego (Thermodynamic and Technological Aspects of the Production of a Nitrided Layer on Iron and Steels in Gas Nitriding Processes)*; Wydawnictwo Politechniki Poznańskiej: Poznań, Poland, 2002. (In Polish)
23. Holst, A.; Kante, S.; Leineweber, A.; Buchwalder, A. Mechanism of Layer Formation during Gas Nitriding of Remelted Ledeburitic Surface Layers on Unalloyed Cast Irons. *Metals* **2023**, *13*, 156. [CrossRef]
24. Dyson, F.J. Electron spin resonance absorption in metals. II. Theory of electron diffusion and the skin effect. *Phys. Rev.* **1955**, *98*, 349. [CrossRef]
25. Bojanowski, B.; Kaczmarek, S.M. Electron spin resonance of $FeVO_4$. *Mater. Sci. Pol.* **2014**, *32*, 188–192. [CrossRef]

26.   Kaczmarek, S.M.; Fuks, H.; Berkowski, M.; Głowacki, M.; Bojanowski, B. EPR properties of concentrated NdVO$_4$ single crystal system. *Appl. Magn. Res.* **2015**, *46*, 1023–1033. [CrossRef]

27.   Kaczmarek, S.M.; Michalski, J.; Leniec, G.; Fuks, H.; Frączek, T.; Dudek, A. Applying the FMR technique to analyzing the influence of nitriding on the magnetic properties of steel. *Materials* **2022**, *15*, 4080. [CrossRef] [PubMed]

28.   Crangle, J.; Fogarty, A.; Taylor, M.J. Weak ferromagnetism in 'non-magnetic' austenitic stainless steel. *J. Magn. Magn. Mater.* **1992**, *111*, 255–259. [CrossRef]

29.   Jian, Z.; Kumar, N.P.; Zhong, M.; Yemin, H.; Reddy, P.V. Structural, Magnetic and Dielectric Properties of Bi$_{0.9}$Re$_{0.1}$FeO$_3$ (Re = La, Sm, Gd and Y). *J. Supercond. Nov. Magn.* **2015**, *28*, 2627–2635. [CrossRef]

30.   Borgioli, F.; Galvanetto, E.; Bacci, T. Low temperature nitriding of AISI 300 and 200 series austenitic stainless steels. *Vacuum* **2016**, *127*, 51–60. [CrossRef]